Local atomic order and element-specific magnetic moments of Fe_3Si thin films on MgO(001) and GaAs(001) substrates

B. Krumme,[1,*] C. Weis,[1] H. C. Herper,[1] F. Stromberg,[1] C. Antoniak,[1] A. Warland,[1] E. Schuster,[1] P. Srivastava,[1,†] M. Walterfang,[1] K. Fauth,[2] J. Minár,[3] H. Ebert,[3] P. Entel,[1] W. Keune,[1,4] and H. Wende[1]

[1]*Fachbereich Physik and Center for Nanointegration Duisburg-Essen (CeNIDE), Universität Duisburg-Essen, Lotharstraße 1, D-47048 Duisburg, Germany*

[2]*Experimentelle Physik IV, Physikalisches Institut, Universität Würzburg, Am Hubland, D-97072 Würzburg, Germany*

[3]*Institut für Physikalische Chemie, Universität München, Butenandtstraße 5-13, D-81377 München, Germany*

[4]*Max-Planck-Institut für Mikrostrukturphysik, Weinberg 2, D-06120 Halle, Germany*

(Received 21 May 2009; revised manuscript received 8 September 2009; published 9 October 2009)

We investigated the magnetic as well as the structural properties of Fe_3Si films on GaAs(001)-(4×6), GaAs(001)-(2×2), and MgO(001) by x-ray magnetic circular dichroism (XMCD) and Mössbauer spectroscopy. From the XMCD spectra we determine averaged magnetic moments of $1.3-1.6\mu_B$ per Fe atom on the different substrates by a standard sum-rule analysis. In addition, XMCD spectra have been calculated by using the multiple-scattering Korringa-Kohn-Rostoker method which allows the site-specific discussion of the x-ray spectra. The Mössbauer spectra show a highly ordered and stoichiometric growth of Fe_3Si on MgO while the growth on both GaAs substrates is strongly perturbed, probably due to diffusion of substrate atoms into the Fe_3Si film. Therefore, we have studied the influence of Ga or As impurities on the magnetic properties of Fe_3Si by calculations using coherent-potential approximation within the Korringa-Kohn-Rostoker method. For selected impurity concentrations additional supercell calculations have been performed using a pseudopotential code (VASP).

DOI: 10.1103/PhysRevB.80.144403 PACS number(s): 75.50.Bb, 78.70.Dm, 75.70.Ak, 76.80.+y

I. INTRODUCTION

Since the idea of using the spin of the electrons in addition to their charge as a carrier of information, tremendous effort has been made to create spin-polarized currents in semiconducting materials. One approach is to make use of spin injection, where an electric current is spin polarized by a ferromagnetic electrode from which it is injected into a semiconducting material.[1–3] Strong support for this approach results from the possibility of combining such devices with the existing semiconductor technology. However, there are still many difficulties to overcome before such spintronic devices may finally be established. For a high efficiency in the spin-injection process the ferromagnetic electrode should exhibit a high degree of spin polarization and a perfect interface with the semiconductor.[1] In recent studies, Fe_3Si on GaAs turned out to be a promising ferromagnet-semiconductor combination. Spin injection has successfully been demonstrated with an efficiency of 3%.[4] As the quality of the interface directly influences the spin injection, a better understanding of the correlation between structure and magnetic properties at the interface is necessary to fulfill the task of improving the spin injection.

Fe_3Si is a binary Heusler-type compound. Such Heusler compounds are theoretically predicted to exhibit half-metallic behavior involving a high degree of spin polarization up to 100%.[5,6] However, a spin polarization of $45\pm5\%$ is reported so far.[7] Ordered Fe_3Si crystallizes in a $D0_3$ structure which is described by four interpenetrating fcc lattices[8] whereas randomly distributed Fe and Si atoms lead to a B2 structure. In perfectly ordered Fe_3Si each fcc sublattice is occupied by only one element, i.e., three sublattices are occupied by Fe atoms and one is occupied by Si atoms (Fig. 1). This crystal structure leads to two inequivalent Fe sites: Fe atoms on sites *B* are surrounded by eight nearest-neighbor Fe atoms yielding a magnetic moment of $2.2\mu_B$ per atom.[9] Fe atoms on *A* sites are surrounded by four nearest-neighbor Fe atoms and four Si atoms exhibiting a magnetic moment of $1.35\mu_B$ per atom.[9] As a further consequence of the different surroundings, Fe atoms on different sites have different hyperfine fields which can be resolved by conversion electron Mössbauer spectroscopy (CEMS).[8] The lattices of Fe_3Si and GaAs(001) match almost perfectly (lattice mismatch 0.1% with $Fe_3Si[001]\|GaAs[001]$). Epitaxial growth has been carefully studied in detail.[10–12] In contrast, on MgO a lattice mismatch of 5.2% occurs when Fe_3Si grows rotated by 45°

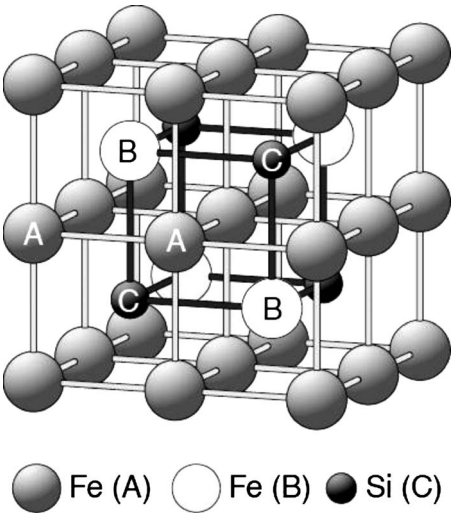

FIG. 1. $D0_3$ structure of bulk Fe_3Si with Fe atoms on inequivalent lattice sites *A* and *B* and Si atoms on site *C*.

on MgO(001), i.e., $Fe_3Si[001]\|MgO[110]$.[13,14] With a Curie temperature of 840 K (Ref. 15) Fe_3Si allows for operation at room temperature (RT). In comparison to pure Fe/GaAs(001) its interface is thermally more stable.[16] Both are crucial facts for the final application in devices.

In the present paper, we take a closer look at the correlation between chemical ordering and magnetic properties in thin films of Fe_3Si. We present our combined x-ray absorption spectroscopy (XAS) and Mössbauer studies for Fe_3Si on GaAs in comparison to MgO. We use Fe_3Si on MgO(001) for comparison as a quality standard for which we know that Fe_3Si films grow highly ordered on this substrate. CEMS allows us to characterize the chemical ordering of the Fe_3Si films and to determine the hyperfine field distributions site dependent. Complementary, the XMCD spectroscopy reveals the averaged magnetic moment per Fe atom. In addition, XAS and XMCD spectra have been calculated within multiple-scattering theory. From the calculations we obtain site-specific spectra, densities of states, and magnetic moments. Furthermore, we have studied the influence of Ga or As impurities on the magnetic properties of Fe_3Si since we gained evidence of an interdiffusion of substrate atoms into the Fe_3Si film on GaAs from our CEMS measurements.

II. EXPERIMENTAL ASPECTS

Films of 80 Å Fe_3Si [57 monolayer (ML)] (Ref. 17) were deposited in an UHV chamber at a base pressure of 1×10^{-10} mbar on three different substrates: MgO(001), Ga-terminated GaAs(001)-(4×6), and As-terminated GaAs(001)-(2×2). The Fe_3Si films on MgO and GaAs-(4×6) were prepared simultaneously so that the growth conditions for both samples were identical. Before introducing the substrates into the preparation chamber, we cleaned them with propanol, the GaAs additionally with acetone, and dried them in a stream of N_2. To obtain the GaAs-(4×6) surface reconstruction, the substrate was sputtered with 500 eV Ar^+ ions while being heated up to a temperature of 870 K for 90 min. For the GaAs-(2×2) surface reconstruction an As-capped GaAs substrate was heated up to 820 K for 10 min. No contamination of the surface with O or C was detectable via Auger spectroscopy after this procedure.

The two elements Fe and Si were coevaporated at a substrate temperature of $T_S=520$ K from a resistively heated crucible and by electron-beam deposition, respectively. For the CEMS measurements, ^{57}Fe isotopes were deposited instead of natural Fe. Figure 2 shows the reflection high-energy electron diffraction (RHEED) we used to monitor the Fe_3Si film growth on GaAs-(4×6) (right column) and MgO (left column). Both pattern sets consist of three pictures comparing the crucial phases of the Fe_3Si growth. The substrate reflections of MgO and GaAs-(4×6) are shown at the top of the columns and were measured along the $[1\bar{1}0]$ direction of Fe_3Si. On MgO the substrate reflections directly change into $Fe_3Si(001)$ reflections within the first ML. This indicates a layer-by-layer growth from the very beginning. In contrast, on GaAs-(4×6) the substrate reflections totally vanish when the deposition is initiated. The first Fe_3Si reflections appear

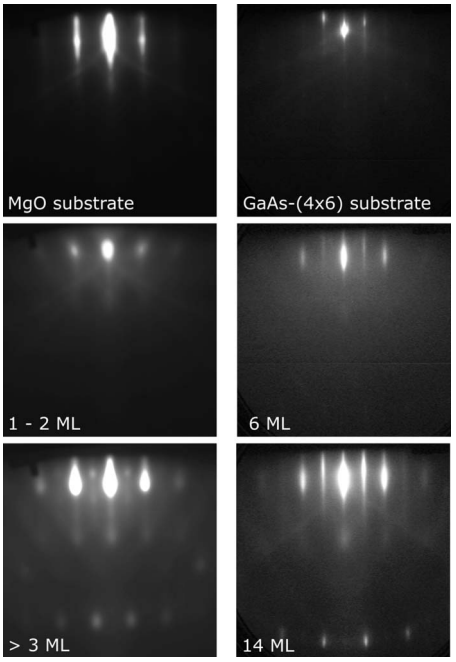

FIG. 2. RHEED patterns of $Fe_3Si(001)$ film growth on MgO(001) (left column) and GaAs-(4×6) (right column) measured during growth at 520 K with an electron energy of 15 keV. The growth was observed along the [100] direction of MgO and along the $[1\bar{1}0]$ direction on GaAs. Both correspond to the $[1\bar{1}0]$ direction of Fe_3Si (details see text).

only at a film thickness of about 6 ML indicating a coalescence of the initial islands at that thickness. Recent *in situ* studies by real-time x-ray diffraction find that the growth of Fe_3Si on GaAs(001) begins with islands of 6 atomic layers height and changes to a two-dimensional layer-by-layer growth at about 14 atomic layers.[10] Finally, the samples were capped with 20 Å Au for transportation to the measuring chamber.

We investigated XAS and XMCD spectra at the dipole beamline PM3 at BESSY in Berlin, Germany. We detected the XAS at the Fe $L_{2,3}$ edges in total-electron yield mode by measuring the drain current of the sample. For a simultaneous determination of the incoming photon flux I_0 we recorded the photocurrent of a Au mesh in the incident beam. The dichroic spectra were obtained by changing the direction of the magnetization while the helicity of the circularly polarized synchrotron radiation remained constant. The easy axis of magnetization is in plane along the [100] direction of the Fe_3Si.[18] Thus, we measured at grazing incidence with an angle of 20° between the photon wave vector and the surface of the sample. The sum rules derived by Thole *et al.*[19] and Carra *et al.*[20] were applied to determine spin- and orbital-resolved magnetic moments from the dichroic signal of the Fe atoms in the sample. This method reveals magnetic moments per Fe atom averaged over the two different Fe sites. Before normalizing the XAS to unity, the measured spectra have been normalized to the incoming photon flux and corrected for a small linear background. Saturation effects have been considered as described, e.g., in Refs. 21–23.

CEMS was applied to characterize the chemical ordering of the Fe_3Si films. We used a ^{57}Co source embedded in a Rh

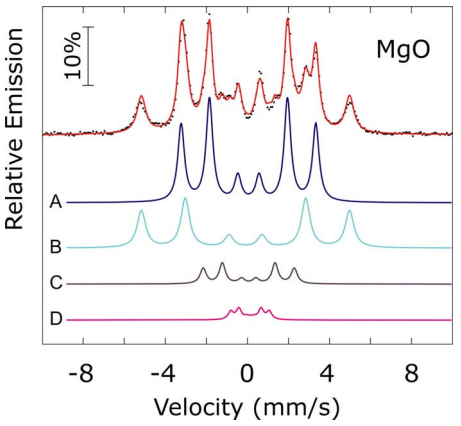

FIG. 3. (Color online) CEMS of bulklike $Fe_3Si(001)$ film (57 ML) on MgO(001) least-squares fitted by four sextets.

matrix. The samples were mounted in a gas flow proportional counter with a He-5% CH_4 mixture. The CEMS were all measured in zero external field at room temperature. Since the surroundings of Fe atoms of type A, Fe(A), differs from that of type B atoms, Fe(B), their hyperfine magnetic fields are different. Therefore, the individual Mössbauer spectra of the two types of Fe atoms have a different splitting of the lines in the corresponding sextet. Hence, the experimental spectrum will mainly show the superposition of two such sextets,[8] as is illustrated in Fig. 3 for a bulklike Fe_3Si film on MgO(001). The spectrum was least-squares fitted using the computer code NORMOS.[24] The four-fitted subspectra at the bottom (shifted downward for clarity) represent the two sextets of Fe atoms on the two inequivalent sites whereas the two additional subspectra with smaller intensity originate from a not perfectly ordered $D0_3$ crystal structure. The solid line above is the sum of the sextets, fitting well the experimental data that are represented by the solid circles. It is thus possible to clearly distinguish the two dominant inequivalent Fe sites in a Mössbauer spectrum by fitting sextets with different hyperfine fields to the experimental data. The hyperfine field, B_{hf}, and isomer shift (relative to bulk bcc Fe at room temperature), δ of the A-site and B-site subspectra in Fig. 3 have been determined as $B_{hf}(B)=30.78\pm0.02$ T, $\delta(B)=0.090\pm0.002$ mm/s, $B_{hf}(A)=19.96\pm0.01$ T, and $\delta(A)=0.250\pm0.001$ mm/s. The errors given are the statistical errors. These values are in good agreement with those reported in the literature for bulk Fe_3Si alloy.[25]

For a more detailed analysis and a clearer inspection of the interface properties, the Mössbauer spectra were least-squares fitted in two steps: (i) spectra of highly chemically ordered Fe_3Si films can be fitted satisfactorily by a procedure described by Arita *et al.*,[26] subspectrum (1) in Fig. 4. (ii) To account for disorder at the interfaces of the films, an additional subspectrum [subspectrum (2) in Fig. 4] with a hyperfine field distribution $P(B_{hf})$ is required in the case of GaAs(001) substrates.

Within the first step of the fitting routine the sites are randomly occupied by Fe and Si atoms. The fit to the experimental data is obtained by varying this site occupancy and calculating the corresponding CEM spectra. Long-range, $S(D0_3)$, S(B2), and short-range, $\alpha(1)$, $\alpha(2)$, order parameters

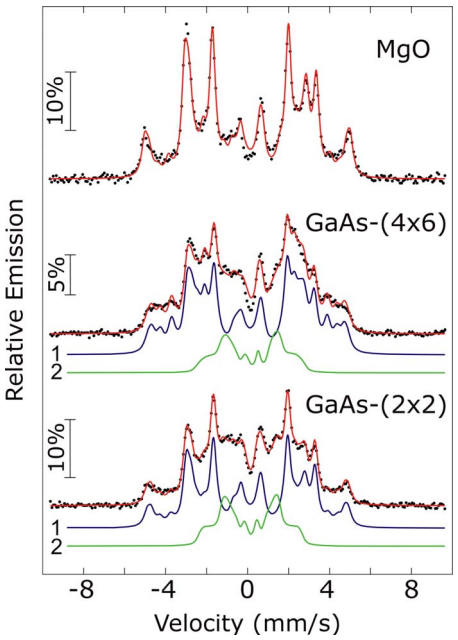

FIG. 4. (Color online) Measured CEMS (solid circles) of 57 ML Fe_3Si on different substrates at RT together with fitting curves (lines) as described in the text.

are computed from the occupancy of Fe sites with different nearest and next-nearest Si atoms that leads to the best matching simulated spectrum [subspectrum (1)]. If after this first step a considerable part of the CEM spectra cannot be satisfactorily fitted, an additional subspectrum with a hyperfine field distribution [subspectrum (2)] is used to describe the remaining part in the second step, accounting for an additional, non-Fe_3Si-like Fe phase.

III. COMPUTATIONAL ASPECTS

The theoretical XMCD data are obtained from *ab initio* calculations employing the spin-polarized relativistic Korringa-Kohn-Rostoker (KKR) method as implemented in the SPR-KKR code.[27–29] For the exchange-correlation functional the local-density approximation in the parametrization of Vosko *et al.*[30] has been used. For the calculations of the corresponding XAS and XMCD spectra we used an expression based on Fermi's golden rule which was implemented within the SPR-KKR code.[27] For the KKR calculations we have used an angular momentum expansion up to $l_{max}=2$ and a k-point mesh of $22\times22\times22$ (which corresponds to 843 irreducible k points). In order to study the influence of Ga and As impurities on the magnetic structure of Fe_3Si KKR calculations within the coherent-potential approximation (CPA) as well as supercell calculations employing the VASP code and the projector-augmented wave pseudopotentials[31,32] have been performed. For the latter, orthorhombic supercells with 32 atoms have been used in which one or two Fe atoms of type B have been replaced by Ga or As, respectively. The generalized gradient correction (PW91) (Ref. 33) has been used for the supercell calculations. A mesh of $15\times8\times4$ k points and an energy cutoff of 381.3 eV have been used. The

TABLE I. Chemical order parameters for 57 ML Fe_3Si on different substrates, determined from a comparison of measured CEMS and CEMS simulations as described in the text.

Substrate	S($D0_3$)	S(B2)	$\alpha(1)$	$\alpha(2)$
Theoretical values	1	0.67	−0.33	−0.33
MgO	0.83 ± 0.07	0.52 ± 0.12	−0.23	−0.31
GaAs-(4×6)	0.68 ± 0.002	0.32 ± 0.1	−0.09	−0.38
GaAs-(2×2)	0.78 ± 0.03	0.42 ± 0.12	−0.38	−0.40

experimental lattice constant of Fe_3Si $a=5.65$ Å has been used for all calculations containing Fe_3Si neglecting possible tetragonal distortions which may occur if Fe_3Si is grown on a substrate. In order to ensure that small tetragonal distortions have no significant influence on the magnetic moments of the system we have performed KKR-CPA calculations in which the c/a ratio is varied by $\pm 5\%$ keeping the volume fixed. The maximum change in the orbital (spin) moments is less than 2% (4%). However, the average change in magnetic moments is smaller being about 1.5%. This holds also in the presence of impurities. Relaxation of the lattice constant due to the Ga or As impurities has been neglected so far.

IV. RESULTS

The characterization of the chemical ordering of the Fe_3Si films with CEMS is shown in Fig. 4. Solid circles represent the experimental data. The lines represent the subspectra (1) and (2) used for the fitting as described above, and the total spectrum. On MgO it was adequate to fit the experimental data with a calculated spectrum for nearly perfectly ordered Fe_3Si and the fitting was completed after the first step as described above. The spectra of Fe_3Si films on GaAs-(4×6) and GaAs-(2×2) had to be fitted with two subspectra in order to account for the nonperfect order in the film. Spectrum (1) is calculated following the work of Arita *et al.*[26] and spectrum (2) is the additional subspectrum with a distribution of magnetic hyperfine fields representing a non-Fe_3Si phase, which we attribute to an imperfect interface. This could be related to an interdiffusion at the interface between Fe_3Si and the substrate. Hsu *et al.*[34] were able to ascribe this interdiffusion to Ga atoms. Such an interdiffusion of nonmagnetic impurity atoms would result in a lower magnetic ordering and a reduced magnetic Fe moment. The chemical order parameters that we obtained from our analysis are summarized in Table. I. In the first row of the table, the expected values for perfectly ordered Fe_3Si are given. In real samples the order can be perturbed by the interface to the substrate or a capping layer, thus lowering the order parameters. From the CEM spectra of the Fe_3Si film on MgO we obtained parameters S($D0_3$) and S(B2) which are reduced by 17% and 22% compared to the ideal values. In the case of GaAs substrates the change in the order parameters becomes even more dramatic resulting in a deviation of up to 50%. Comparison of the CEM spectra of the Fe_3Si films on the Ga-terminated GaAs-(4×6) and the As-terminated GaAs-(2×2) surfaces reveals more pronounced peaks in the

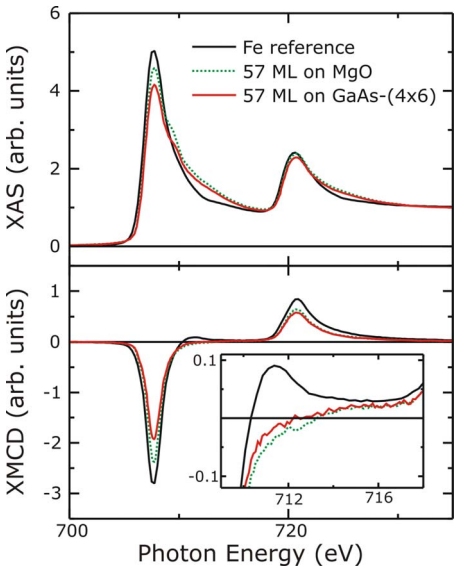

FIG. 5. (Color online) Normalized XAS (top) and XMCD (bottom) spectra measured at the Fe $L_{2,3}$ edges of 57 ML Fe_3Si on MgO and GaAs-(4×6) compared to the spectra of a bulklike Fe sample as a reference. The inset shows an enlargement of the XMCD signal between the $L_{2,3}$ edges. The spectra were measured at RT.

case of GaAs-(2×2) indicating a better chemical ordering on GaAs-(2×2) than on GaAs-(4×6). In the case of GaAs-(4×6) subspectrum (2) has a spectral area of $20.8 \pm 0.2\%$ whereas for GaAs-(2×2) this value becomes $29.6 \pm 0.2\%$. This leads us to the conclusion that the disorder in the films on GaAs-(4×6) is due to Ga interdiffusion at the interface and that on GaAs-(2×2) the interdiffusion is due to Ga as well as As atoms.

^{57}Fe CEMS of Fe_3Si does not directly yield information about the value of the magnetic moment of the Fe atoms. Thus, we applied the XMCD spectroscopy to determine spin- and orbital-resolved magnetic moments. Figure 5 shows the XAS as well as the XMCD spectra at the Fe $L_{2,3}$ edges of the Fe_3Si films on MgO and GaAs-(4×6) together with a bulklike Fe film as a reference. The $L_{2,3}$ edges of the XAS spectra are broader for the Fe_3Si films in comparison to the Fe reference. Concurrently, the maximum of the absorption signal at the L_3 edge decreases by ~8% for Fe_3Si on MgO(001) and by ~17% on GaAs-(4×6). Additionally, a shoulder occurs 2 eV above the L_3 edge in the Fe_3Si XAS. However, at the L_2 edge the absorption intensity is nearly unchanged. The broadening as well as the shoulder can be ascribed to a hybridization of Fe and Si atoms in the lattice. Such a feature has been observed in other Heusler systems by Kallmayer *et al.*[35] The white lines of Fe_3Si on GaAs-(4×6) and GaAs-(2×2) in Fig. 6 exhibit no obvious difference indicating a very similar electronic structure of Fe_3Si on various surface reconstructions.

For a detailed study of the structure the electronic density of states, DOS, and the XAS of bulk Fe_3Si have been calculated, allowing a site-specific analysis of the spectra. From the DOS it is obvious that the two types of Fe atoms have a different electronic structure. Atoms of type B have nearly the same DOS as bulk Fe whereas the A-type atoms show a

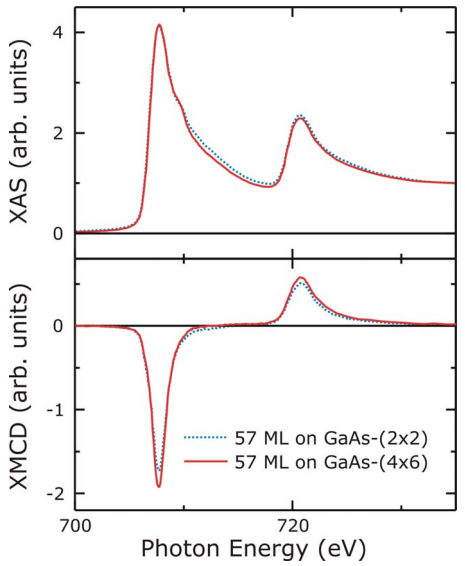

FIG. 6. (Color online) Normalized XAS (top) and XMCD (bottom) measured at RT at the Fe $L_{2,3}$ edges of 57 ML Fe_3Si on GaAs-(2×2) and GaAs-(4×6).

completely different behavior, see Fig. 7, which is related to the fact that in the latter case only half of the nearest neighbors are Fe atoms. This is in agreement with previous investigations.[36,37] The different properties of the two Fe types are also translated to the x-ray spectra, see Fig. 8. Similar to the experimentally observed shoulder (cf. Fig. 5) a small bump P between 2 and 6 eV is observed in the theoretical spectrum. However, this feature occurs only in the L_3 peak of the Fe(A) atoms and seems to be caused by a hybridization of an Fe *d* orbital with a *s* state of Si, see Fig. 8. The spectrum of the Fe(B) atoms looks very similar to that of bulk Fe showing no P-like structure at the L_3 peak. Furthermore, from Fig. 8 it is obvious that the spectra of the two types of Fe are slightly shifted against each other, i.e., the maxima of the Fe(A) L_3 peak occurs about 0.25 eV above the

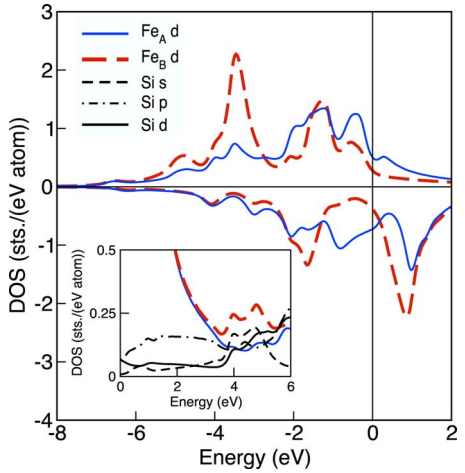

FIG. 7. (Color online) Calculated spin-resolved density of states of Fe_3Si. The inset shows the total (not spin-resolved) DOS of the region above the Fermi energy (E_F=0) being relevant for the calculation of XMCD spectra.

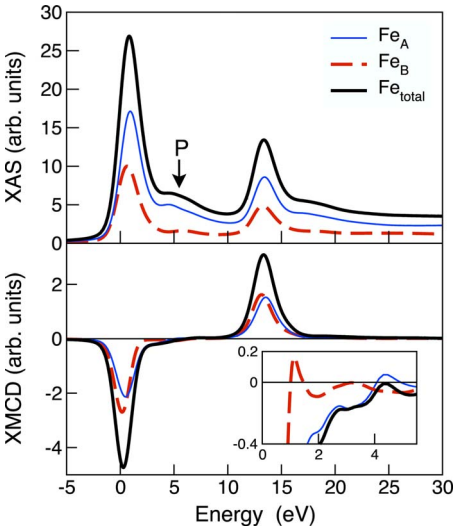

FIG. 8. (Color online) Calculated XAS (top) and XMCD (bottom) spectra of Fe in bulk Fe_3Si (E_F=0). The inset is an enhancement of the energy region between the L_3 and L_2 peak. In order to make these tiny features visible we disclaim smoothing of the data.

L_3 peak of the Fe(B) atoms. Such a shift of the XAS spectra could not be observed directly in the experiment because the energy difference is smaller than the linewidth of the L_3 peak. The different position of the two XAS is accompanied by a change in the number of *d* holes. The atoms of type A have less *d* holes compared to bulk Fe, namely, $\Delta h = -0.24$ whereas the number of holes for Fe(B) remains unchanged compared to bulk Fe. The difference between the A and B Fe atoms becomes also obvious from the XMCD. If we disclaim Gaussian broadening to simulate the broadening caused by the experimental measurement, a tiny positive signal occurs in case of Fe(B) (see inset of Fig. 8) which is known from bulk bcc Fe cf. Fig. 5.

Comparing the XMCD signal of the Fe reference with those of the Fe_3Si films in Figs. 5 and 6 no features can be found which allow a deconvolution of the magnetic contributions of the different Fe sites. Only a decrease in the XMCD intensity can be observed for Fe_3Si films. For Fe_3Si on MgO the XMCD signal corresponding to the L_3 edge is decreased by ~15%. In the case of Fe_3Si on GaAs-(4×6) this difference becomes ~31%. Even a change in the surface reconstruction to GaAs-(2×2) results in a further reduction in the XMCD signal to ~38%. The diminution of the XMCD goes along with diminishing magnetic moments obtained from the sum-rule analysis shown in Table. II. The magnetic moment on MgO calculated with the sum rules is $1.6\mu_B$ and is in very good agreement with results from the literature.[9] On GaAs we obtained decreased moments. Whereas the magnetic moment on GaAs-(4×6) is reduced by ~6%($1.5\mu_B$), which is within the estimated error bar of 10% for the sum rules, on GaAs-(2×2) we obtained a moment decreased by ~19%($1.3\mu_B$). Taking a closer look at the XMCD signal between the $L_{2,3}$ edges reveals a change in the spectral trend. The inset of Fig. 5 shows an enlargement of this feature. Contributions to the XMCD signal in this energy range are ascribed to *sp*-hybridized states or *spd*-wave mixing.[23] Pure Fe has a clear positive XMCD signal in this

TABLE II. Total averaged magnetic moment per Fe atom and ratio of orbital moment m_l to spin moment m_s as obtained from sum-rule analysis for 57 ML Fe_3Si. We estimate the error bar in the order of 10%.

Substrate	m_{tot} in μ_B	m_l/m_s
Fe reference	2.2	0.04
MgO	1.6	0.09
GaAs-(4×6)	1.5	0.06
GaAs-(2×2)	1.3	0.11

range, in contrast to Fe_3Si, for which the signal almost completely vanishes. So one can conclude that the *sp* hybridization in Fe_3Si is different to that of pure Fe. We attribute this difference to the effect of the Si bonding with Fe which happens by 4*s* electrons which can be also seen in the inset of Fig. 7 at an energy of 4 eV.

A possible explanation for the reduced magnetic moments in Fe_3Si/GaAs(001) is the diffusion of As or Ga atoms from the substrate in the ferromagnet. The influence of alike diffusion is studied by placing Ga and As impurities in bulk Fe_3Si. Although the lattice mismatch between Fe_3Si and the GaAs substrate is rather small this should be a reasonable model. We have used two different methods to investigate the influence of impurities on the magnetic properties of Fe_3Si, namely, CPA method where Fe and impurity atoms partially share the same lattice site and supercell calculations in which single Fe atoms are replaced by Ga or As atoms. Impurity concentrations up to 10% have been taken into account, whereby it turned out from our calculations that Ga and As preferably occupy Fe(*B*) sites. Impurities on the low moment Fe(*A*) sites are less important because one has to effort more energy to place the impurities on Fe(*A*) instead of Fe(*B*) sites. In order to figure out the size of possible impurity concentrations in Fe_3Si the mixing energy

$$E_{\mathrm{mix}} = E_{\mathrm{Fe}_{3-x}\mathrm{Y}_x\mathrm{Si}} - (3-x)E_{\mathrm{Fe}} + xE_Y + E_{\mathrm{Si}} \qquad (1)$$

has been calculated, which determines whether the alloy $Fe_{3-x}Y_xSi$ with *Y* being Ga or As is stable against decomposition. In Eq. (1) the energies on the right side correspond to the calculated ground-state energies of the elements, which is a reasonable choice in case of Ga. For As the situation is more complex because there exist a huge number of Fe-As alloys such that the alloy may decompose in one or more of these alloys instead of its elements. However, Eq. (1) gives evidence of the amount of the impurity concentration. In case of Ga the mixing energies are negative if the impurity concentration does not exceed 3.3%. The As-containing alloy seems to be stable for all investigated concentrations, which may be related to the above-mentioned problem of the proper choice of the decomposition components.

In case of 3.33% Ga or As the energy difference between the impurities sitting on Fe(*B*) or Fe(*A*) sites amounts to 138.5 and 182.7 meV/f.u., respectively. The same trend is observed for the supercell calculations. An impurity concentration of 4.17% (i.e., one Fe atom is replaced by an impurity) of Ga (As) on Fe(*A*) sites leads to a 157.4 meV/f.u.

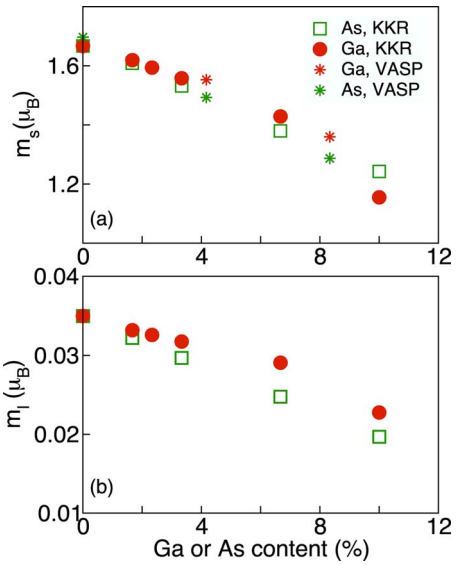

FIG. 9. (Color online) (a) Spin and (b) orbital magnetic moments of $Fe_{3-x}Y_xSi$ (Y=As,Ga) depending on the impurity concentration *x* in percent. Results marked by circles and squares obtained from KKR-CPA calculations. Stars denote the magnetic moments derived from supercell calculations (VASP) for $Fe_{(24-n)}Y_nSi_8$ (Y=As,Ga) with n=1,2.

(237.8 meV/f.u.) higher energy compared to impurities on Fe(*B*) sites. Independent which method—CPA or supercells—has been used the magnetic moments decrease in equal measure with increasing impurity concentration, see Fig. 9. Assuming an impurity concentration of 3.33% the average spin moment is reduced by $0.12\mu_B$ ($0.15\mu_B$) in case of Ga (As). The absolute values of the orbital moments obtained from plain spin density-functional calculations are always too small compared to experiment. However, we observe the same trend as for the spin moments, i.e., the orbital moments are slightly smaller compared to the value obtained for Fe_3Si. However, the above discussed results suggest that the magnetic moments of Fe_3Si/GaAs-(4×6) and −(2×2) are related to alloy formation at the interface. An impurity concentration of 3.3% seems to be sufficient to decrease the average magnetic moment by about $0.1\mu_B$, which is of the same magnitude as the change in the measured magnetic moments, see Table II. The even smaller magnetic moment of the (2×2)-reconstructed surface may be related to additional As diffusion, which can be larger as compared to Ga diffusion. Although the absolute value of the magnetic moments is decreased by Ga and As impurities this has only minor influence on the spin polarization. The spin polarization is mainly determined by the difference of the majority $N^{\uparrow}(E_F)$ and minority density of states $N^{\downarrow}(E_F)$ at the Fermi level E_F,

$$P = \frac{N^{\uparrow}(E_F) - N^{\downarrow}(E_F)}{N^{\uparrow}(E_F) + N^{\downarrow}(E_F)}. \qquad (2)$$

From Eq. (2) we obtained a spin polarization of −42.3% for pure Fe_3Si which is close to the value known from the literature.[7] For $Fe_{2.9}Ga_{0.1}Si$ (impurity concentration=3.33%)

the spin polarization still amounts to −36.8% which is close to the value obtained for bulk Fe_3Si. The high degree of spin polarization as well as the weak dependence between spin polarization and interface quality in the system Fe_3Si/GaAs(001) make this system interesting for further studies.

V. SUMMARY

In summary, we have investigated structural and magnetic properties of Fe_3Si on GaAs and MgO by combining XMCD and Mössbauer measurements with calculations within multiple-scattering theory. From CEMS we gain evidence for chemical disorder of Fe_3Si on GaAs substrates. Measured and calculated XMCD spectra match well even in details of the fine structure between the L_3 and L_2 edges, thus yielding well agreeing averaged Fe moments. As one result of the calculations we obtain the different contributions to the XMCD from Fe on the two inequivalent sites, which are not distinguishable in the experimental spectra. To investigate the influence on the magnetic properties by diffusion of substrate atoms, we have carried out KKR calculations considering Ga and As impurities with various concentrations. Concluding, our results indicate an interdiffusion at the interface of Ga atoms from the substrate, although the spin polarization of Fe_3Si is not dramatically affected.

ACKNOWLEDGMENTS

We thank U. v. Hörsten for help with sample preparation and CEMS measurements. We gratefully acknowledge support during our beamtimes by BESSY staff. Financially supported by DFG (SFB 491 and SFB 445) and BMBF (Grant No. 05 ES3XBA/5).

*Corresponding author; bernhard.krumme@stud.uni-due.de
†Permanent address: Nanostech Laboratory, Indian Institute of Technology Delhi, New Delhi 110 016, India.

[1] G. Schmidt and L. W. Molenkamp, Semicond. Sci. Technol. **17**, 310 (2002).
[2] S. Hövel, N. C. Gerhardt, M. R. Hofmann, F.-Y. Lo, A. Ludwig, D. Reuter, A. D. Wieck, E. Schuster, H. Wende, W. Keune, O. Petracic, and K. Westerholt, Appl. Phys. Lett. **93**, 021117 (2008).
[3] S. Hövel, N. C. Gerhardt, M. R. Hofmann, F.-Y. Lo, D. Reuter, A. D. Wieck, E. Schuster, W. Keune, H. Wende, O. Petracic, and K. Westerholt, Appl. Phys. Lett. **92**, 242102 (2008).
[4] A. Kawaharazuka, M. Ramsteiner, J. Herfort, H.-P. Schönherr, H. Kostial, and K. H. Ploog, Appl. Phys. Lett. **85**, 3492 (2004).
[5] R. A. de Groot, F. M. Mueller, P. G. van Engen, and K. H. J. Buschow, Phys. Rev. Lett. **50**, 2024 (1983).
[6] V. N. Antonov, D. A. Kukusta, A. P. Shpak, and A. N. Yaresko, Condens. Matter Phys. **11**, 627 (2008).
[7] A. Ionescu, C. A. F. Vaz, T. Trypiniotis, C. M. Gürtler, H. García-Miquel, J. A. C. Bland, M. E. Vickers, R. M. Dalgliesh, S. Langridge, Y. Bugoslavsky, Y. Miyoshi, L. F. Cohen, and K. R. A. Ziebeck, Phys. Rev. B **71**, 094401 (2005).
[8] M. B. Stearns, Phys. Rev. **168**, 588 (1968).
[9] W. A. Hines, A. H. Menotti, J. I. Budnick, T. J. Burch, T. Litrenta, V. Niculescu, and K. Raj, Phys. Rev. B **13**, 4060 (1976).
[10] V. M. Kaganer, B. Jenichen, R. Shayduk, W. Braun, and H. Riechert, Phys. Rev. Lett. **102**, 016103 (2009).
[11] V. M. Kaganer, B. Jenichen, R. Shayduk, and W. Braun, Phys. Rev. B **77**, 125325 (2008).
[12] J. Herfort, H.-P. Schönherr, and K. H. Ploog, Appl. Phys. Lett. **83**, 3912 (2003).
[13] D. Kmiec, B. Sepiol, M. Sladecek, M. Rennhofer, S. Stankov, G. Vogl, B. Laenens, J. Meersschaut, T. Ślezak, and M. Zajkac, Phys. Rev. B **75**, 054306 (2007).
[14] Kh. Zakeri, I. Barsukov, N. K. Utochkina, F. M. Römer, J. Lindner, R. Meckenstock, U. von Hörsten, H. Wende, W. Keune, M. Farle, S. S. Kalarickal, K. Lenz, and Z. Frait, Phys. Rev. B **76**, 214421 (2007).
[15] Y. Nakamura *et al.*, *Landolt-Börnstein*, New Series Vol. III/19c (Springer, Berlin, Germany, 1988).
[16] J. Herfort, H.-P. Schönherr, A. Kawaharazuka, M. Ramsteiner, and K. H. Ploog, J. Cryst. Growth **666-670**, 278 (2005).
[17] We call each layer of atoms in the crystal structure 1 monolayer (ML), i.e. the schematic view in Fig. 1 represents 5 ML in our definition.
[18] K. Lenz, E. Kosubek, K. Baberschke, H. Wende, J. Herfort, H.-P. Schönherr, and K. H. Ploog, Phys. Rev. B **72**, 144411 (2005).
[19] B. T. Thole, P. Carra, F. Sette, and G. van der Laan, Phys. Rev. Lett. **68**, 1943 (1992).
[20] P. Carra, B. T. Thole, M. Altarelli, and X. Wang, Phys. Rev. Lett. **70**, 694 (1993).
[21] R. Nakajima, J. Stöhr, and Y. U. Idzerda, Phys. Rev. B **59**, 6421 (1999).
[22] J. Hunter Dunn, D. Arvanitis, N. Mårtensson, M. Tischer, F. May, M. Russo, and K. Baberschke, J. Phys.: Condens. Matter **7**, 1111 (1995).
[23] W. L. O'Brien and B. P. Tonner, Phys. Rev. B **50**, 12672 (1994).
[24] R. A. Brand, Nucl. Instrum. Methods Phys. Res. B **28**, 398 (1987).
[25] M. B. Stearns, Phys. Rev. **129**, 1136 (1963).
[26] M. Arita, S. Nasu, and F. E. Fujita, Trans. Jpn. Inst. Met. **26**, 710 (1985).
[27] H. Ebert, Rep. Prog. Phys. **59**, 1665 (1996).
[28] The MUNICH SPR-KKR package, version 3.6, H. Ebert *et al.*, http://olymp.cup.uni-muenchen.de/ak/ebert/SPRKKR
[29] H. Ebert, Lect. Notes Phys. **535**, 191 (2000).
[30] S. H. Vosko, L. Wilk, and M. Nussiar, Can. J. Phys. **58**, 1200 (1980).
[31] G. Kresse and J. Furtmüller, Comput. Mater. Sci. **6**, 15 (1996).
[32] P. E. Blöchl, Phys. Rev. B **50**, 17953 (1994).
[33] J. P. Perdew and Y. Wang, Phys. Rev. B **45**, 13244 (1992).
[34] Y. L. Hsu, Y. J. Lee, Y. H. Chang, M. L. Huang, Y. N. Chiu, C. C. Ho, P. Chang, C. H. Hsu, M. Hong, and J. Kwo, J. Cryst. Growth **301-302**, 588 (2007).
[35] M. Kallmayer, H. J. Elmers, B. Balke, S. Wurmehl, F. Emmerling, G. H. Fecher, and C. Felser, J. Phys. D **39**, 786 (2006).

[36] Kh. Zakeri, S. J. Hashemifar, J. Lindner, I. Barsukov, R. Meckenstock, P. Kratzer, Z. Frait, and M. Farle, Phys. Rev. B **77**, 104430 (2008).

[37] N. I. Kulikov, D. Fristot, J. Hugel, and A. V. Postnikov, Phys. Rev. B **66**, 014206 (2002).